Enhancing the Potential of Hydrothermal Waxes from Polyethylene: Product Characterization and Insights from Solvent Effects

Guocheng Wang[1], Haoyu Xiao[1], Małgorzata Sieradzka[2], Zuzanna Prus[2], Małgorzata Wilk[2], Aneta Magdziarz[2], Yingquan, Chen[1], Haiping Yang[1], Jiawei Wang[3], Yang Yang[1*]

Affiliation

[1]*State Key Laboratory of Coal Combustion, Huazhong University of Science and Technology, Wuhan, Hubei 430074, China*

[2]*AGH University of Krakow, Mickiewicza 30 Av., 30-059 Krakow, Poland*

[3]*School of Engineering and Applied Sciences, Swansea University, Swansea SA1 8EN, UK*

[*]Corresponding author, e-mail: y.yang100@outlook.com (Y. Yang)

Abstract

The accumulation of plastic waste poses a serious environmental challenge, and their traditional disposal methods became insufficient. The autoclave hydrothermal processing method, employing supercritical water as a solvent, offers notable advantages for plastic pyrolysis, including high conversion efficiency and superior product yield.The main objective of this study is to enhance the characterisation of wax product from hydrothermal conversion of PE plastic, thereby facilitating research into heavy hydrocarbons outside the gasoline and diesel range. Thus, the impact of temperature and polar solvent on the product distribution have been profoundly examined. The findings demonstrate that at temperatures below 420°C, the hydrothermal wax displays a hardness comparable to paraffin and is insoluble in conventional solvents. The addition of polar solvents enhanced the efficiency of PE chain scission, whereas the presence of oxygen broadened the product distribution. Ethanol induced chemical cyclisation in the hydrothermal wax, resulting in the formation of liquid aromatic compounds (25.96%). In contrast, acetic acid resulted in the softening of the wax, leading to the production of a higher proportion of light hydrocarbons (83.2%). The characteristics of hydrothermal wax were analysed using thermogravimetric analysis (TG), gas chromatography-mass spectrometry (GC-MS), Fourier transform infrared spectroscopy (FTIR), proton nuclear magnetic resonance (^{1}H NMR) and carbon nuclear magnetic resonance (^{13}C NMR). Finally, the molecular formulas were validated through the use of heteronuclear multiple bond correlation (HMBC) spectroscopy.

Keywords: plastic recycling, hydrothermal conversion, hydrothermal wax, heavy hydrocarbons,

1. Introduction

Versatile properties of plastic materials, such as durability, light weight, chemical resistance, and relatively low cost of manufacture made them applicable in many different industrial branches, especially in engineering, packaging and automotive sectors(Andrady and Neal, 2009). Polymer materials are primarily derived from natural resources such as crude oil and natural gas. Therefore, their formation contribute to serious environmental concerns, such as depletion of non-renewable natural resources, greenhouse gas emissions, and the pollution from plastic waste (Nayanathara Thathsarani Pilapitiya and Ratnayake, 2024). In 2022, the worldwide production of plastics exceeded 400.3 million tonnes, which is 2.4% higher than in the year before, and 200 times more than in 1950s (Statistica, 2024). As both production and the use of plastic materials over the past few decades has significantly increased, so does the environmental issues associated with plastics. Moreover, a growing number of studies highlights increasing environmental contamination by microplastics (Prus and Wilk, 2024), especially in marine habitats, as around 85% of marine litter originated from land sources is plastics (Derraik, 2002). It has been proved that the presence of microplastics can adversely affect the life processes of organisms causing a long-term risk to ecosystem (Chang et al., 2022; Sarma et al., 2022). From another point of view, the chemical and physical properties of plastics might suggest their usefulness in terms of energy recovery.

The Higher Heating Value (HHV) of synthetic polymers ranges from 20 to 46 MJ/kg(Al-Salem and Lettieri, 2010; Barbarias et al., 2018; Huang et al., 2019; Qiao et al., 2018) which confirms their significant energy content. This makes plastics a valuable feedstock for waste-to-energy (WTE) technologies, where they can be processed to generate electricity or heat. Considering the increasing market size of plastic materials, there is a need to develop an effective plastic recycling technology, with beneficial energy recovery for economic and ecological sustainability (Wang et al., 2023).

The primary methods of plastic waste disposal are landfill and incineration. However, the inherent stability of plastics makes them difficult to degrade naturally, while incineration generates a significant number of particles and organic derivatives that contribute to atmospheric pollution (Zhang et al., 2021). Although numerous regulations have been implemented and proposed, the mechanical recycling rate for plastics remains relatively low, amount to less than 7% in US, which generates the most plastic waste in global scale (Hendrickson et al., 2024; Khatun et al., 2021). Consequently, identifying a technological pathway to process efficiently substantial quantities of plastic waste has emerged as a prominent research topic (Maqsood et al., 2021).

Currently in use, conventional treatment methods including incineration, landfill, and mechanical recycling, are insufficient and inadequate for converting plastic waste into high-value-added products, unlike thermal conversion (Al-Salem and Lettieri, 2010). Thermochemical treatment of plastics, such as hydrothermal conversion has gained recent attention, as it does not generate gaseous pollutants, and enables to obtain products with a concentrated carbon number distribution by controlling the reaction conditions (e.g. temperature, reaction time, or catalyst) (Cheng et al., 2023; Fivga and Dimitriou, 2018). Products from hydrothermal conversion of plastic encompass gaseous hydrocarbons and light oils, among others. In addition, the extent of product enrichment can be enhanced by introducing specific catalysts, facilitating the production of high-value-added products, including fuel oil and carbon nanotube materials (Liu et al., 2023; Yang et al., 2024). However, plastics initially yields heavy hydrocarbons ($> C_{20}$) during the chain-breaking process, which are cracked into products such as small molecule gases and carbon deposits. In addition, at ambient temperature, heavy hydrocarbons tend to solidify into hydrothermal waxes (Artetxe et al., 2013).

The primary component of plastic-derived, hydrothermal waxes is olefin(Ding and Hesp, 2021), commonly utilized as an industrial filler in asphalt to lower the asphalt compaction temperature and as a feedstock in refineries for fuel and chemical production (Abdy et al., 2022; Bray et al., 2020). Plastic waxes may also contain small amounts of alcohols, acids, esters and olefins internally, and are in solid state at room temperature. Polyethylene waxes, with high thermal stability and low manufacturing cost, can be used as additives to blend with asphalt to reduce asphalt viscosity and enhance the high temperature performance and aging resistance of composites. They can also be used as feedstock in the cracking process of refineries for the production of fuels and chemicals, which is conducive to the realization of waste utilization and the reduction of environmental pollution (Li et al., 2023). Hydrothermal waxes contain lighter hydrocarbon molecules (boiling point range of 150–200 °C), unsaturated bonds and aromatic compound components that are highly irritating to the skin, which limits the application of waxes. Although during distillation process the lighter hydrocarbons are removed, further upgraded utilization of hydrothermal waxes still needs to be explored (Patil et al., 2024).

Plastic-derived waxes are readily produced during hydrothermal conversion, but the lack of separation methods of oil and solid phases well as high value application pathways are the major concern of this technology. Currently, the research on hydrothermal waxes concentrates on increase of the product yields and complex processes. The mechanism of plastic hydrothermal conversion indicates that high-yield waxes can be produced without requiring high-temperature environments or metal-loaded catalysts(Al-Salem and Dutta, 2021). Nevertheless, current research lacks characterisation of plastic hydrothermal waxes and exploration of solvent effects in hydrothermal conversion. Conventional analytical methods can only measure the relative content of each heavy hydrocarbon in hydrothermal waxes, but are not sufficient to quantify the individual substance products, let alone understand their structure and carbon chain length.

Therefore, the main aim of this research is to fill a gap in current knowledge regarding the characteristics of wax obtained by PE hydrothermal conversion, as one of the most commonly used plastic. The hydrothermal conversion of PE at different temperatures was carried out and the effect of the addition of different solvents (H_2O_2, C_2H_5OH, CH_3COOH at 1, 20 and 100% concentrations) on the wax properties were examined.

2. Materials and Methods

2.1. Materials

Pure Polyethylene (PE) was used as the main feedstock for the hydrothermal conversion. It was selected due to its extensive usage in the manufacture of plastic packaging, such as bottles, which subsequently enter the marine environment, contributing to the accumulation of marine waste plastics. The PE material was purchased from a commercial supplier, ensuring consistent quality and purity for the experimental trials. Chemicals: Ethanol (C_2H_5OH), Hydrogen peroxide (H_2O_2), and Acetic acid (CH_3COOH) were purchased from China National Pharmaceutical Group Chemical Reagent Co. Ltd. 0.22 μm filters were provided by General Electric Biotechnology Co. Ltd.

Raw material and produced waxes were subjected to elemental analysis using a Vario Micro cube elemental analyser (purchased from Elementar, Germany) in accordance with the Chinese national standard (GB/TGB/T 18338.2-2001).

2.2. Hydrothermal conversion

The autoclave reactor with capacity of 500 mL, manufactured by Parr Instruments was employed to conduct hydrothermal conversion under operating pressures up to 34.5 MPa and temperatures up to 500 °C. It is equipped with a pressure meter, safety rupture discs, inlet and outlet gas valves, valves for the sampling of liquid, cooling coils, and thermocouple sleeves with J-joints. The scheme of the reactor is depicted in Figure 1.

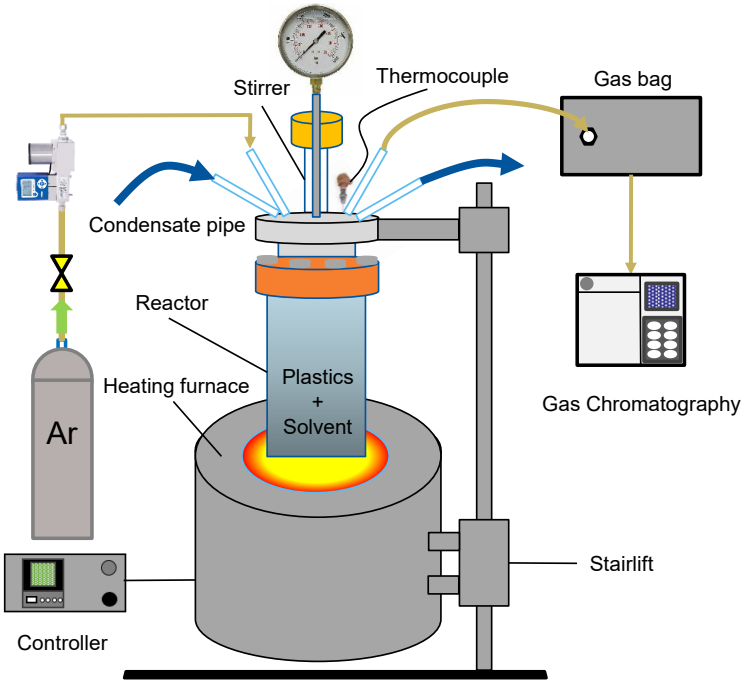

Fig. 1. Scheme of the hydrothermal reactor.

The following temperatures were selected for the hydrothermal conversion: 410, 420, 425, 430, 435 and 440 °C. In each experimental trial, 20 g of PE and 40 mL of deionised water or solvent were used. In order to investigate the impact of diverse solvents on the wax production from PE, several solutions were studied. C_2H_5OH was employed as a polar solvent for the purpose of washing and potentially dissolving certain impurities. H_2O_2 was utilised due to its well-documented oxidative properties, serving to facilitate the removal of organic contaminants or to enable specific reactions during the post-treatment phase. CH_3COOH was used as a mild acid, with the potential to act as a process catalyst or as neutraliser, depending on the requirements of the reaction. In order to investigate the impact of diverse solvents on wax production, a series of experiments were conducted, wherein the following percentages of solvents were employed: 1%, 20%, and 100%. Following the assembly of the reactor, three purges with argon were conducted to eliminate residual air within the kettle. Thereafter, the pressure was adjusted to 0.62 MPa. The reactor was subsequently heated to the set temperature and maintained at that temperature for a period of 30 min. Once the process was completed, the cooling water valve was opened in order to rapidly reduce the temperature of the reactor to the

room temperature. The pressure was recorded, and then the exhaust port was opened to allow the collection of the gas products. The kettle was transferred to a beaker and weighed. The liquid and solid hydrothermal products were separated by filtration with filter paper, and the water and oil phases were separated by a glass separatory funnel. The oil that had formed a film on the inside of the funnel was carefully removed with cotton and weighed. This measure was included in the final oil weight. The total mol of gas was first calculated using the ideal gas law based on the temperature and pressure after the reaction, the mol percentage of each gas was calculated based on the gas chromatograph, and then the mass of each gas was calculated separately and added up to give the total gas yield.

2.3. Analytical methods

GC-MS

The liquid products were subjected to analysis by gas chromatography/mass spectrometry (7890B/5977A, Agilent). For the purpose of sample preparation, 50 mg of the sample was dissolved in 5 mL of dichloromethane, mixed and filtered through a 0.22 μm filter membrane. The GC-MS injector was maintained at 280 °C with a split ratio of 20:1. The samples were separated using an HP-5 MS capillary column (30 m × 0.25 mm × 0.25 μm, Agilent). The oven was set to maintain a temperature of 40 °C for 2 min, after which it was heated to 200 °C at a heating rate of 5 °C/min. Finally, the oven was heated to 280 °C at a heating rate of 10 °C/min and maintained for 2 min. The products were identified according to the National Institute of Standards and Technology Mass Spectral Library 2017 Version (NIST17.L library).

NMR

Nuclear magnetic resonance (^{1}H NMR and ^{13}C NMR) spectroscopy was performed using deuterobenzene at 600 MHz on a Bruker Avance II 600 spectrometer with relaxation times of 2 s and 5 s and 128 and 1024 scans, respectively. Heterogeneous Multiple Bond Correlation (HMBC) was employed for detection of the wax products structure. The analysis was performed

in deuterated benzene on a Bruker Avance II 600 spectrometer at 600 MHz with a relaxation time of 2 s and 16 scans. For each sample, 100 mg of wax was dissolved in 0.6 mL of deuterated benzene and filtered through a 0.22 μm PTFE syringe filter.

FTIR

Identification of functional groups in wax samples was conducted using Fourier transform infrared spectroscopy (FTIR) manufactured by a PerkinElmer ATR-FTIR (Thermo Nicolet IS5) with a spectral range of 4000-600 cm^{-1} and 256 scans with a resolution of 4 cm^{-1}.

TG

The thermal stability of hydrothermal waxes and oils was analysed using a thermogravimetric (TG) analyser (STA-449F3 NETZSCH). Approximately 10 mg of each sample was placed in crucible and then placed in the oven to be heated from 20 °C to 550 °C at a rate of 10 °C/min in a nitrogen rate of 60 ml/min.

GC

The composition of the gaseous products was identified using a dual-channel gas chromatograph (Panna A91, Panna Instruments). The gas chromatography was equipped with a thermal conductivity detector (TCD) and a flame ionization detector (FID), where the following carrier gases were introduced: helium (He) and nitrogen (N_2), respectively. The TCD separated the following compounds: H_2, N_2, O_2, CO_2, CH_4 and CO on a Porapak molecular sieve column and a 5A zeolite molecular sieve column, while olefins and alkanes were separated on an Al_2O_3/KCl capillary column in FID. The column temperature was 80 °C and held for 4 min, then heated to 150 °C at a heating rate of 10 °C/min and held for 6 min.

3. Results and Discussion

3.1. Influence of process temperature on the wax production

Hydrothermal experiments of PE were carried out at various temperatures, namely 410, 420 , 430 and 440 °C, to evaluate its effect on the wax yield and characterise the obtained products.

Experiments at 410, 420 and 430 °C provided mainly solid products. At 440 °C, it was observed that only the liquid products were obtained. After collecting and observing the wax/oil products from these initial tests, additional experiments at 425 °C and 435 °C were conducted. The product derived at 425 °C was found to give the most visually satisfactory results, indicating a more favourable conversion and product consistency. That is why, this particular product, PE wax produced at 425 °C, was chosen for further analysis. Figure S1 shows the wax/oil products generated from the hydrothermal experiments at all selected temperatures.

The yields of the solid, liquid and gas products for all studied temperatures are shown in Figure 2(a). For the temperature of 410 °C, almost only solid products were obtained, and no gas was detected. The solid products consist mainly of wax and no liquid products were identified. As the temperature increased, the liquid products were produced. For instance, at 435 °C and 440 °C the products consisted of 96.7% and 93.9% liquid, respectively, where no wax was produced. The solid yields of the products derived at 420 °C and 425 °C were similar to each other, and amounted to 98.8%. Based on visual inspection of the consistency of the sample produced at 425 °C, this one was chosen as the most satisfactory. Concluding, at 425 °C was proven to be the most suitable process temperature for wax production. Figure 2 b illustrates the effect of process temperature on gas production. According to the presented results, C_2 hydrocarbons were the primary gas components, with the highest yield determined for sample derived at 440 °C, with amount of 796.2 μmol/g, and the lowest found for sample produced at 410 °C, with amount of 70.2 μmol/g. It might be concluded that an increase in process temperature favours the formation of gas components, which indicates that higher process temperature provides the release of a higher amounts of volatiles from raw material. The total lower heating value (LHV) of the gas at 440 °C was determined to be 53.4 kJ/kg.

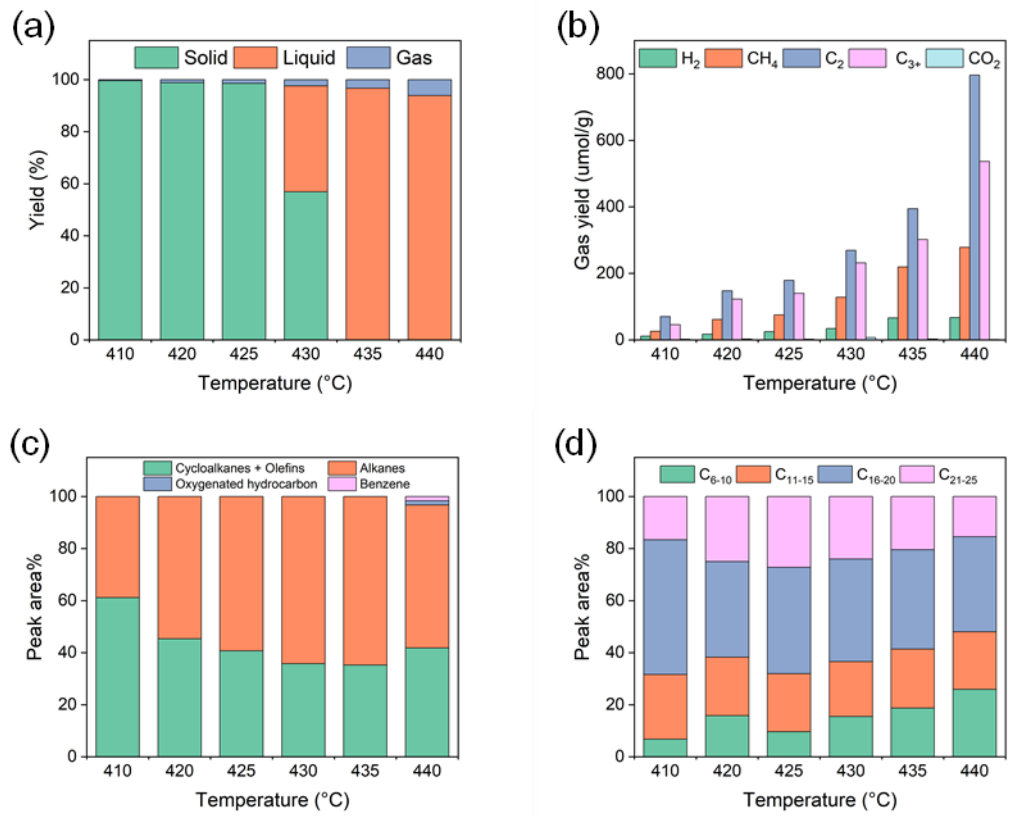

Figure 2. Characteristics of hydrothermal conversion of PE at different temperatures: (a) product yield; (b) gas composition; (c) distribution of products by structure; (d) distribution of products by carbon number.

The GC-MS results are presented in Figure 2c, d. It is observed that liquid samples contain hydrocarbon chains ranging from C_6 to C_{25}. It can be seen that the liquid oils are of good quality and have a distinct carbon number distribution, which can be classified into the following groups: C_6-C_{10}, C_{11}-C_{15}, C_{16}-C_{20} and C_{21}-C_{25}. Additionally, the results were categorised into following groups: cycloalkanes plus olefins, alkanes, oxygenated hydrocarbons and benzene. It is worth noting that the solid samples produced at 410 and 420 °C could not be fully dissolved in dichloromethane. Therefore, the results at these two temperatures could not be used for comparison, and additional TG analyses were performed for the undissolved solids. As shown in Fig. 2c, the waxes/oils obtained above 420 °C consisted mainly of chain alkanes, cycloalkanes and olefins, ranging from 35.3 – 41.8 wt.%. Sample of 410 °C have the highest

238 percentage of cycloalkanes and olefins (59.2%). This phenomena can be attributed to high
239 number of Brønsted acid sites in the sample, which facilitates the breakdown and aromatisation
240 of polyolefins during hydrothermal conversion resulting in the generation of a higher yield of
241 aromatic hydrocarbons(Liu et al., 2025). Small amounts of benzene rings and oxides were
242 observed to be produced at 440 °C, with 1.6 wt.% and 1.7 wt.%, respectively. As shown in
243 Figure 2c, the waxes at 425 °C were mainly composed of heavy hydrocarbons with yields of
244 37.6 wt.% and 25 wt.% for C_{16}-C_{20} and C_{20}-C_{25}, respectively, and only 8.9 wt.% for C_6-C_{10}. As
245 the temperature increases to 440 °C, the yield of C_{20}-C_{25} gradually decreases to 15.4 wt.% and
246 the yield of C_6-C_{10} gradually increases to 25.9 wt.%. Results for compounds up to C_{20} can be
247 categorised as double-bond olefins. Some of the compounds from C_7 to C_{17} are single bond
248 paraffins(Norouzi et al., 2024).
249 The thermal cracking of waxes at different temperatures and waxes insoluble in
250 dichloromethane at 410 and 420 °C were additionally investigated via thermogravimetric
251 analysis (Figure 3). Decomposition of samples occurred in a one broad step, starting at
252 temperature of 100 °C and ending at 500 °C (Figure 3a, b). The initial weight loss up to 100 °C
253 may be related to release water from the sample. For most studied cases, except samples 435
254 °C and 440 °C, the main weight loss occurred at temperature range of 380 – 510 °C related to
255 the decomposition of coke residue(Kongngoen et al., 2023). The highest weight loss rate was
256 observed at temperature 476 °C with 58.6 % weight loss for 410 °C sample, 458 °C with 80.2%
257 weight loss for 425 °C sample, 459 °C with 78.1% weight loss for 420 °C sample, 458 °C with
258 98.2% weight loss for 430 °C sample, 286 °C with 54.3% weight loss for sample 435 °C and
259 230 °C with 41.1% weight loss for 440 °C sample. Samples of 410 °C, 425 °C, 420 °C and 430
260 °C decomposed at higher temperatures due to the higher degree of crystallinity and the presence
261 of a long-chain polymer structure in comparison to other samples(Norouzi et al., 2024). The
262 higher processing temperature resulted in a material with a more fluid consistency, as evidenced

by the photographic documentation of the samples. This phenomenon led to an increased weight loss during thermogravimetric analysis. Consequently, the thermal stability of these samples is lower than that obtained in lower temperature.

The weight loss of insoluble waxes in dichloromethane at 410 and 420 °C occurs at 280 °C, as presented at Figure. 3c, d. The GC-MS results (Figure 2c, d) demonstrate a distribution of products up to C_{25}, while one of the main components are alkanes. Usually, wax decomposition at temperature lower than 225 °C are attributed to degradation of alkanes with low molecular mass(Kongngoen et al., 2023). The undissolved 410 °C and 420 °C samples showed the mass loss of 92.8 wt.%, 80.2 wt.% and at 480 °C. Consequently, the samples obtained at lower temperatures were mainly hard, heavy fractions insoluble in methylene chloride, which confirm the experimental records.

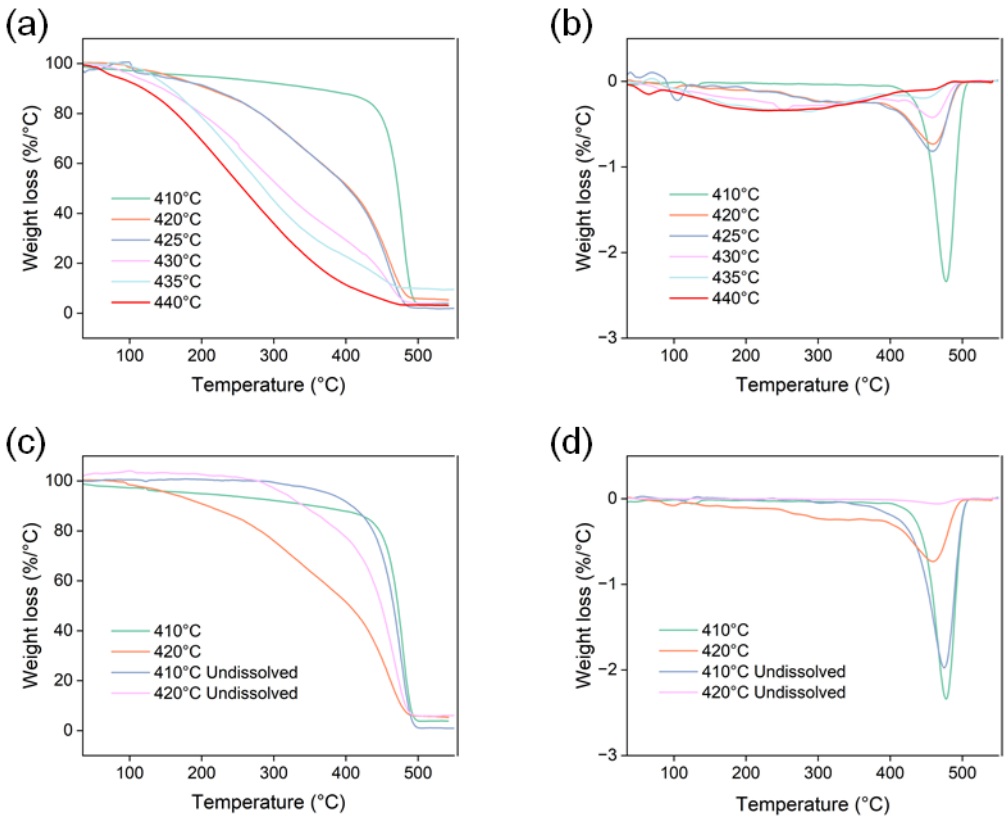

Figure. 3. TG and DTG curves of wax products: (a), (b) in different temperatures; (c), (d) 410 and 420 °C wax samples insoluble in methylene chloride.

The GC-MS results do not accurately reflect the percentage of unsaturated bonds in the olefins and the carbon number distribution of the products. Therefore, waxes and oils were analysed using ^{1}H NMR to determine the changes in the distribution of unsaturated H, methylene H, and methyl H content with temperature and the structural formulae determined by heteronuclear multiple bond correlation (HMBC). As shown by the GC-MS results, almost no benzene was produced at all temperatures, so deuterated benzene was chosen as the solvent. The peak positions of aromatic H and aliphatic H were 6–9 ppm and 0.5–6 ppm, respectively, and the solvent peak position of deuterobenzene was 7.16 ppm (Babij et al., 2016).

The ^{1}H NMR analyses of the products at all temperatures are presented in Figure. S2, which showed only the aliphatic part. The peak positions of -CH_3 substituents were in the range of 0.5–1 ppm, -CH_2-substituents were in the range of 1–1.5 ppm, -CH-substituents were in the range of 1.8–2.3 ppm, and -CH=CH- substituents were in the range of 1–2 ppm (Rudyk et al., 2023). The relative amount of each substituent was obtained by integrating the peaks over the peak area and by averaging the carbon chains, employing a modification of the Cookson and Smith method (Speight et al., 2011). Carbon chain length was determined as the ratio of the intensity of the peak area of the 3-fold methylene group to that of the methyl group plus the number of methyl groups at each end. This method can only be used for straight-chain alkanes, so the products were elementally analysed before the calculations, as shown in Table S1. The products contain minimal quantities of oxygen (O) and nitrogen (N), with the majority of their composition consisting of carbon (C) and hydrogen (H). The mole ratios of C and H for the products at PE and 410–440 °C products are 0.47:1, 0.47:1, 0.48:1, 0.55:1, 0.47:1, and 0.54:1, respectively. The mole ratios of C and H for the products at PE and 410–440 °C products are 0.47:1, 0.47:1, 0.48:1, 0.55:1, 0.47:1, and 0.54:1, respectively, which suggests that straight-chain alkanes are preferred to branched-chain, cycloalkane, and aromatics at presented experimental condition.

The results of the FTIR analysis of studied waxes are presented in Figure S3. The primary peaks identified in the FTIR analysis for each studied sample were observed at wavenumbers of 2920, 2850 and 1460 cm^{-1}. These peaks are indicative of long-chain aliphatic hydrocarbons which are the main components of wax (Missau et al., 2018; Movasaghi et al., 2008). The analysis indicated that the absorption frequencies were consistent with those observed in common alkanes, thereby demonstrating similarities between the obtained samples and paraffin waxes (Missau et al., 2018). The absorption bands at 2955, 2870, and 997 cm^{-1} correspond to -CH_3 vibrations, the absorption bands at 2917, 2852, and 910 cm^{-1} correspond to -CH_2- vibrations, and the absorption bands at 1462, 1377, and 720 cm^{-1} correspond to -CH- vibrations, and the three absorption bands correspond to planar asymmetric vibrations and spatially symmetric vibrations, in that order. symmetric vibrations, plane-symmetric vibrations, and space-symmetric vibrations. In addition, the absorption bands at 1640 and 972 cm^{-1} correspond to C=C and C-C vibrations, respectively (Jung et al., 2018). As the process temperature increased, the intensity of the peaks diminished. The highest intensity was observed in 410 °C sample while the lowest intensity was observed in the sample obtained at 440 °C. This indicates that the quantity of identified compounds has decreased which is consistent with the results obtained by ^1H NMR.

The results of the NMR parameters of hydrothermal waxes calculations are shown in Table S2. Notably, as the temperature increases from 410 to 440 °C, the methylene content decreases from 82.82% to 71.48%, while the olefinic, hypromellitic, and methyl content all increase. Therefore, the increase in temperature was favorable to increase the degree of branchedness of the product. The highest carbon chain length of 22.2 was found at 425 °C, the shortest at 440 °C was 14.83, and the carbon chain lengths of 20–22 at 410 and 420 °C were attributed to the fact that the samples obtained at these temperatures dissolved through fully deuterated benzene.

The wax products were analysed by HMBC to clarify further their structure, which provides additional information by correlating hydrogen and carbon nuclei separated by 2–3 covalent bonds. As shown in Figure. 4, the upper axis is the ^{1}H spectrum and the left axis is the ^{13}C spectrum. For the ^{13}C spectrum, the peak at 127.7 ppm has the highest intensity as a solvent peak for deuterobenzene, the peaks between 10–40 ppm have the next highest intensity associated with methyl and methylene, and the peaks at 114.2 and 138.9 ppm have the lowest intensity associated with olefins (Cookson et al., 1985). The position of the peaks can be determined by their position in the carbon chain. Figure 4a, b shows that the ^{1}H peaks at 0.9 ppm and 1.36 ppm were strongly correlated with the ^{13}C peaks at 20–40 ppm and weakly correlated with the ^{13}C peaks at 114.2 and 138.9 ppm. This indicated that the dissolved wax was a straight chain with little branched chains and olefins present. However, it was observed that the ^{1}H peaks at 2.0 and 5.8 ppm were correlated with the ^{13}C peaks at 28.9 and 33.6 ppm, respectively, suggesting the presence of olefins and branched chains in the HMBC plots of waxes at other temperatures. It was noteworthy that the ^{1}H peak at 5.8 ppm showed a weak correlation with the ^{13}C peak at 33.6 ppm due to the low content of the H atom. The position of the olefin in the carbon chain was determined according to the strength of the correlation between the two olefin H. In addition, the ^{13}C peaks at 14.2 and 138.9 ppm showed a stronger correlation with the ^{1}H peak at 1.35-2.0 ppm, especially the strongest correlation with the ^{1}H peak at 2.0 ppm. This finding further validated the presence of olefins and suggested the presence of branched structures near the unsaturated carbon on the carbon chain. The waxes at 425–435 °C have similar structures, but an additional ^{1}H peak at 5.0 ppm can be observed in the 440 °C waxes associated with ^{13}C peaks at 114.2 and 138.9 ppm, suggesting the presence of two unsaturated carbon structures in the carbon chain. The correlation between the peaks at 0.9 ppm and 1.36 ppm in the ^{1}H spectrum and the ^{13}C peaks at 20–40 ppm was further strengthened, indicating increased branching.

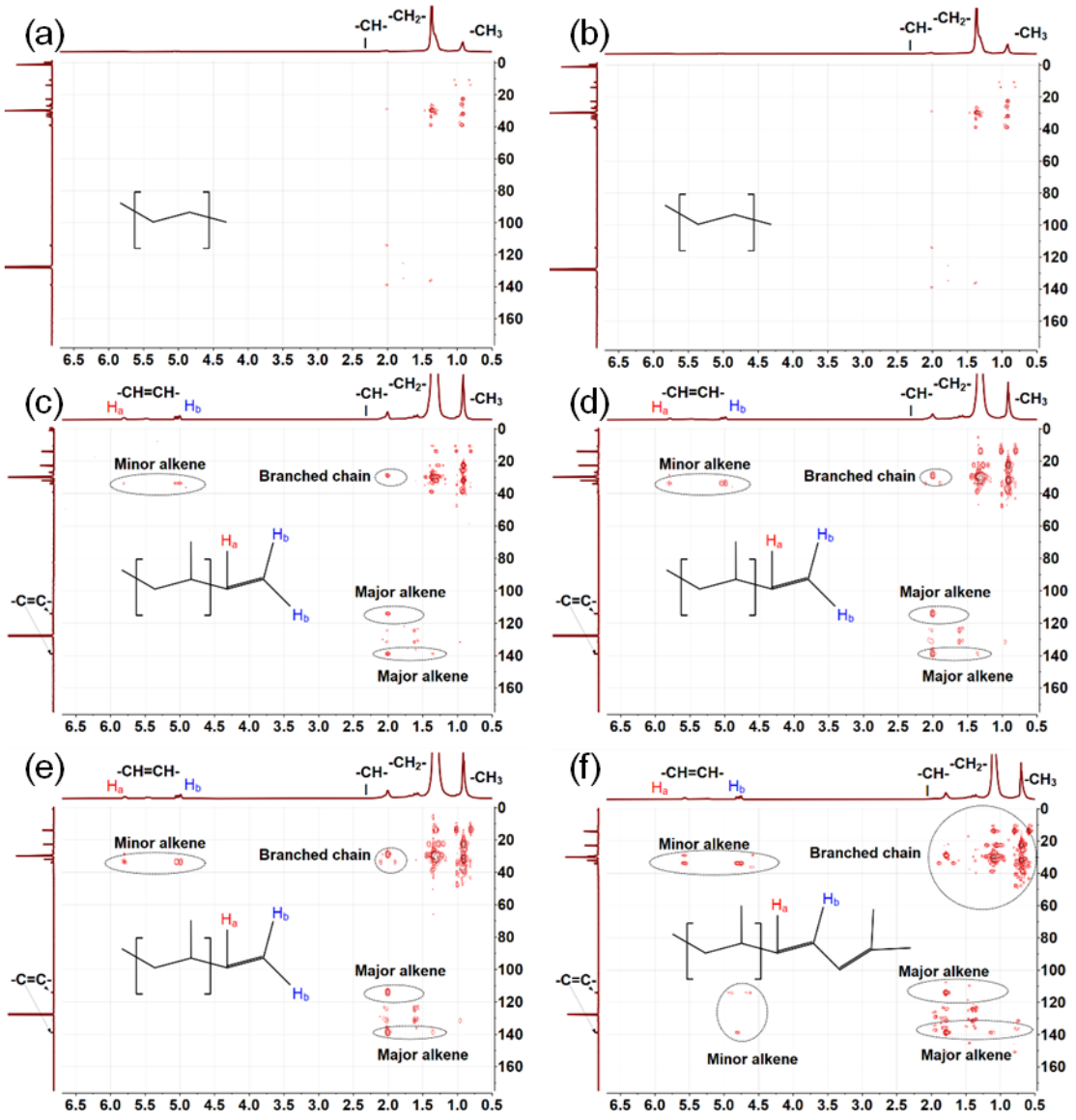

Figure 4. NMR-HMBC plots under hydrothermal wax at different temperatures: (a) 410 ℃, (b) 420 ℃,(c) 425 ℃, (d) 430 ℃, (e) 435 ℃, (f) 440 ℃.

3.2. Influence of solvents additive on the wax production.

3.2.1. Hydrothermal conversion of PE in C_2H_5OH

The yields of the solid, liquid and gas products at different C_2H_5OH additions were shown in Figure. 5a. The higher gas yield was produced as the solvent addition increased. For the 100% C_2H_5OH addition, no solid products were identified, the products consist of 77.8 wt.% liquid and 22.2 wt.% gas. The yield of products for 1% and 20% addition were similar to each other, and the solid products were 98.1 wt.% and 96.2 wt.%, respectively. However, the density of the

20% addition sample was less than the 1% addition sample based on visual inspection. This analysis suggests that the addition of C_2H_5OH favours the hydrothermal conversion of plastics to lower molecular weight hydrocarbons.

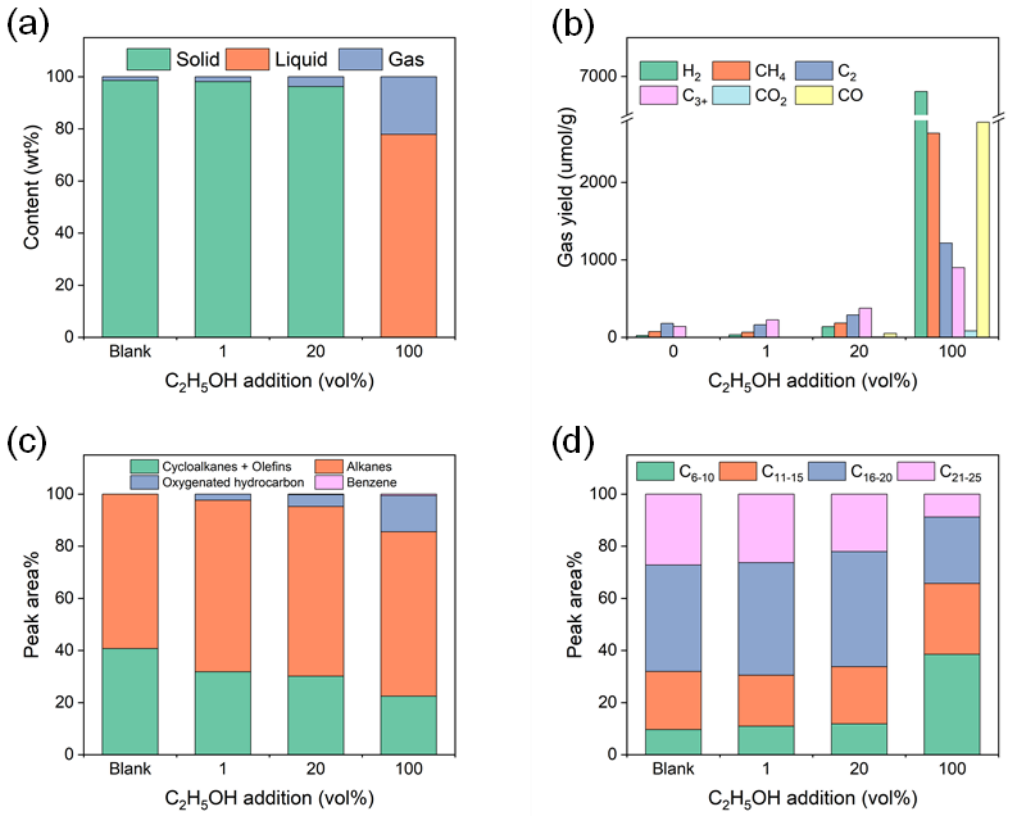

Figure. 5. Hydrothermal conversion of PE at different concentrations of C_2H_5OH: (a) product yield; (b) gas composition; (c) distribution of products by structure; (d) distribution of products by carbon number.

Figure 5b illustrates the effect of solvent addition on gas yield. It is worth noting that alcohol tends to decompose at high temperatures to produce H_2, CH_4 and CO. The results showed that the content of C_2 and C_{3+} hydrocarbons increased with increasing C_2H_5OH content, with yields of 1216.7 µmol/g and 898.8 µmol/g for the samples at 100% C_2H_5OH addition, respectively. The total LHV of this fraction of hydrocarbons was 78.57 kJ/kg. Oxygenated compounds appear in the wax/oil after the addition of C_2H_5OH as shown in Figure 5 c. With the addition of alcohol up to 100 vol%, the oxygenate content gradually increased to 13.8% and a small

amount of aromatic hydrocarbons were produced. The content of chain alkanes did not change significantly, while the content of cycloalkanes and olefins gradually decreased. As shown in Fig. 5 d, at 100% C_2H_5OH addition, the oil consisted mainly of light hydrocarbons with yields of 38.5 % and 27.2 % for $C_{6\text{-}10}$ and $C_{11\text{-}15}$, respectively. However, below 20% C_2H_5OH addition, there was almost no change in the main composition of the waxes, which is consistent with the findings observed visually in the samples.

Samples with the C_2H_5OH addition had an irritant odour, especially in the case of 100% additions. As a result, the curves for TG and DTG were not stable (Figure S5). It was worth noting that the decomposition of the 100% C_2H_5OH sample, started at a temperature of 35 °C and ended at 350 °C in. The results obtained for this sample differed significantly from those obtained for the others. The highest weight loss rate was observed at a temperature of 450 °C with 86.2 wt% weight loss for 1% sample, 446 °C with 91.2 wt.% weight loss for 20% sample, 167 °C with 46.3 wt.% weight loss for 100% sample. Samples of Blank, 1% and 20% C_2H_5OH additions, decomposed at higher temperatures due to the presence of a long-chain polymer structure compared to 100% of C_2H_5OH in the sample. The higher addition of C_2H_5OH resulted in a material with a more fluid consistency, which was in line with the photographic documentation depicted in Figure S4.

The results of FTIR analysis of wax under different C_2H_5OH additions were presented in Figure S6. Higher peak intensities at 1460 cm^{-1} were observed for the samples with 1% and 20% of C_2H_5OH compared to the blank sample, while the relative intensities of other characteristic peaks remained largely unchanged. This indicated that the addition of C_2H_5OH caused an increase of the number of unsaturated bonds. It was noteworthy that the curve of the sample 100% with C_2H_5OH addition exhibits additional peaks at 1120–1010 cm^{-1}, and 3100–3600 cm^{-1}, corresponding to instrumental noise, O-H stretching vibration, and C-O stretching vibration, respectively (Dutta, 2017).

According to the NMR spectra, the weaker peak intensity of $–CH_3$ and $–CH_2–$ was observed for the samples with 1% and 20% C_2H_5OH additions compared to the blank sample in Figure 6. It is noteworthy that the additional peaks appear at 3.5-4 ppm and 7.5-8 ppm in sample with 100%, corresponding to H adjacent to oxygen and H on the benzene ring, respectively. This corroborated the GC-MS results. The relative content of each peak area of the ^1H NMR spectra of the samples at different C_2H_5OH additions were shown in Table S3. The average chain length of the waxes decreased to 18.85 as C_2H_5OH addition increased to 20% and further declined to 10.97 at 100%, accompanied by a significant aromatic hydrogen proportion of 25.96%. The peak at 135 ppm in the ^{13}C NMR spectrum (Figure S7) corresponds to an aromatic structure, correlating with the peak at 7.5 ppm in ^1H NMR but not with the peak at 3.5 ppm. This suggested that the O atom was directly attached to the aromatic ring. Additionally, increasing the addition from 0% to 20% gradually enhanced each correlation signal in the HMBC spectrum, indicating that C_2H_5OH promotes branching, cyclization, and arylation in the wax.

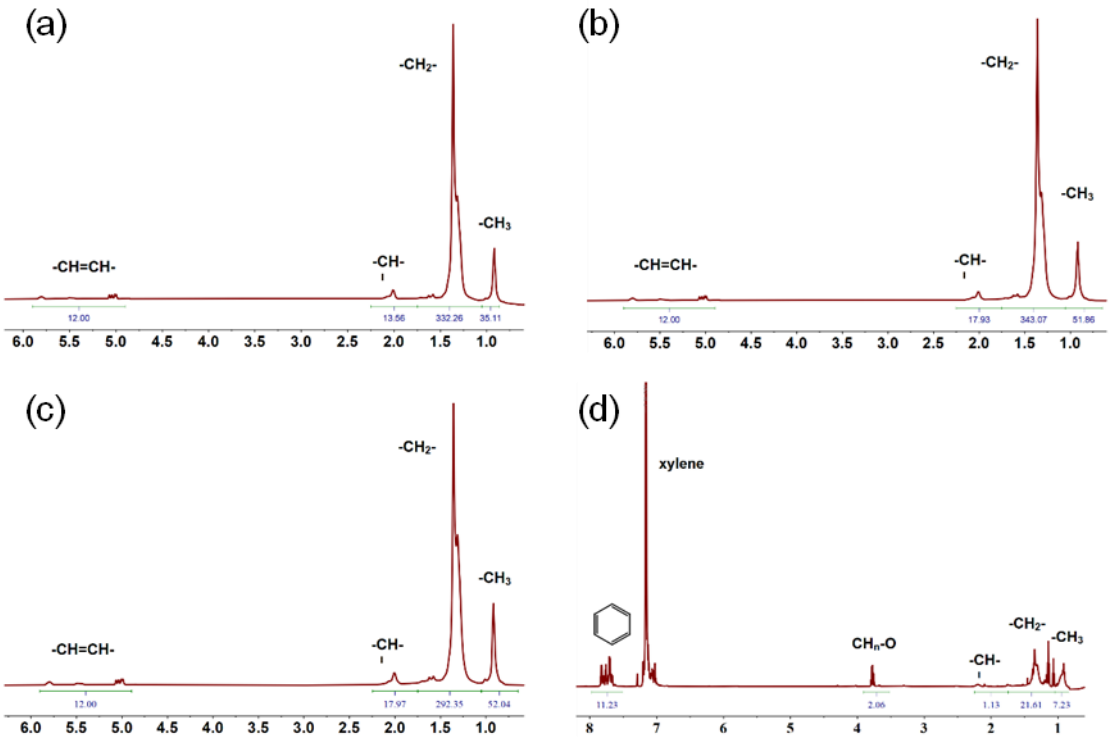

Figure 6. ^1H NMR spectra of hydrothermal waxes obtained with different concentrations of C_2H_5OH (a) 0%, (b) 1%, (c) 20%, (d) 100%.

3.2.2. *Hydrothermal conversion of PE in H_2O_2*

The yields of the solid, liquid and gas products at different H_2O_2 additions were shown in Figure 7. All wax products were visually identified as solids. The wax yield decreased from 98.6% to 78.7 wt.% with 100% solvent addition. Although the thermal decomposition of hydrogen peroxide generated oxygen, Figure 7 b revealed significant CO and CO_2 production, indicating that the carbon source was PE. The concentrations of CH_4, C_2, and C_{3+} hydrocarbons remained stable at 136.3 μmol/g, 373.5 μmol/g, and 287.7 μmol/g, respectively, regardless of the solvent addition. Conversely, H_2 yield increased with the increase of H_2O_2 addition, as the solvent became a new source of H_2 released during hydrothermal conversion. The total LHV of all combustible gases was 30.49 kJ.

The addition of H_2O_2 did not significantly influence the structure of the wax products (Figure 7c) but affected the carbon number distribution (Figure 7 d). The carbon number distributions of the 20% and 100% samples were similar, with $C_{16–20}$ converting to $C_{11–15}$ compared to the blank sample, this resulted in respective contents of 26.1% and 31%. This suggested that oxygen presence led to a more disordered distribution of products below C_{20}, which was consistent with the findings of previous studies (Xu et al., 2023).

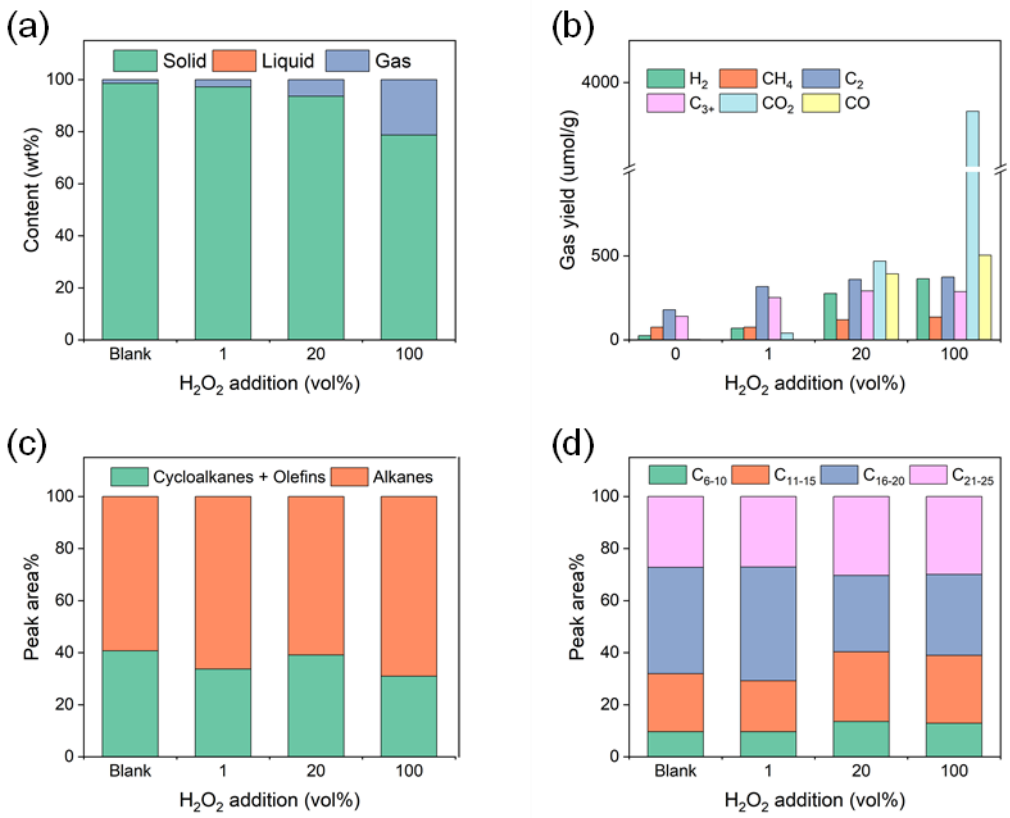

Figure 7. Characteristics of hydrothermal conversion of PE at different concentrations of H_2O_2: (a) product yield; (b) gas composition; (c) distribution of products by structure; (d) distribution of products by carbon number.

The TG and FTIR analyses of the 20% and 100% samples showed a high degree of similarity (Figure S9, S10). The addition of H_2O_2 did not affect the thermal behaviour of the wax, as evidenced by the comparable shapes of the curves on the graph. While the FTIR spectra exhibit main peaks in comparable regions, with varying intensities contingent on the solvent addition. Similarly, the relative peak areas of the characteristic peaks in the ^{1}H NMR spectra (Figure S11) exhibited minimal variation. Statistical results in Table S4 indicated that the addition of hydrogen peroxide reduced the carbon chain length of the wax product from 22.2 to 19.65 while maintaining a straight-chain structure. This was attributed to the presence of oxygen, which promoted the formation of hydrocarbons within the petrol and diesel range. Additionally, visual inspection revealed that the waxes produced with hydrogen peroxide were darker (Figure S8).

3.2.3. Hydrothermal conversion of PE in CH_3COOH

The images displayed in Figure S12 illustrate the waxes obtained through the addition of varying quantities of CH_3COOH. The yields of the solid, liquid and gas products at different CH_3COOH additions were shown in Figure 8 a. Similar to the previous trend, the gas yield increased with higher solvent addition levels. Yields of 96.4 wt.% and 82 wt.% were obtained for the 1% and 20% samples, respectively. Visual inspection revealed that the 20% sample was darker in colour and less dense, while the 100% sample appeared as black liquids. This analysis suggested that the addition of CH_3COOH promoted the hydrothermal conversion of plastics into low molecular weight hydrocarbons.

Figure 8 b showed significant production of CH_4, CO_2, and CO in the 100% sample, those compounds originating from the hydrothermal conversion of CH_3COOH. C_2 and C_{3+} hydrocarbons, as the primary gas components, reached their highest yields at 100% addition, measuring 640 μmol/g and 726 μmol/g, respectively, with a total LHV of 53.21 kJ.

As shown in Figure 8 c, the addition of CH_3COOH did not lead to produce new compounds, but increased the content of chain hydrocarbons from 59.3% to 83.2%. Figure 8 d indicated that the 100% samples primarily consisted of light hydrocarbons, with yields of 17 wt% for $C_{6\text{-}10}$, 31.9 wt.% for $C_{11\text{-}15}$, and only 16.9 wt.% for $C_{21\text{-}25}$.

The thermal cracking of waxes at different additive levels was investigated, as shown in Figure S13. The Blank sample exhibited the highest weight loss of 80.2% at 458 °C, followed by 88% at 455 °C for the 1% sample, 92.1% at 444 °C for the 20% sample, and 44.7% at 239 °C for the 100% sample. The FTIR spectra of the samples were similar, indicating that the addition of CH_3COOH did not alter the structure of the wax products (Figure S14). Figure S15 showed that the hypromellose intensity increased with the addition of CH_3COOH, and a small number of carbonyl peaks appeared in 20% of the samples. Statistics in Table S5 indicated that CH_3COOH reduced the carbon chain length of the wax product from 22.2 to 15.33, for blank sample and

100% sample respectively, and increased branching. This was attributed to the chain scission of PE caused by the acidic environment of CH_3COOH.

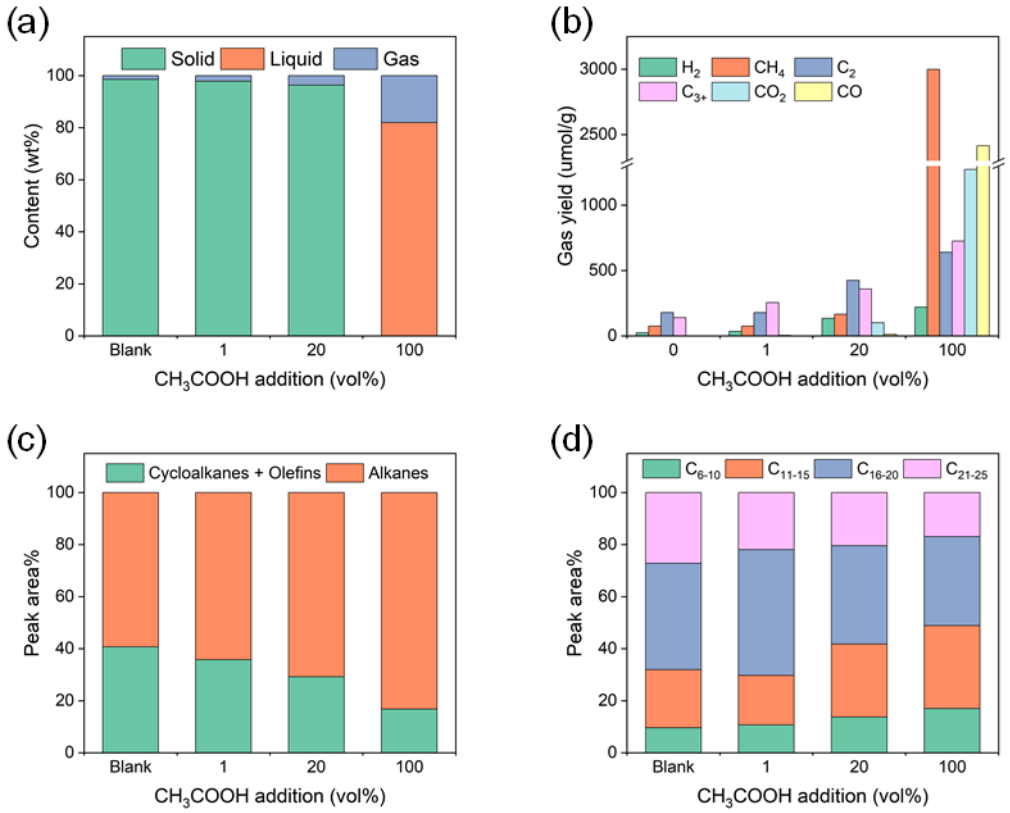

Figure 8. Hydrothermal conversion of plastics at different concentrations of CH_3COOH: (a) product yield; (b) gas composition; (c) distribution of products by structure; (d) distribution of products by carbon number.

4. Conclusions

This study is focused on the characteristics of hydrothermal wax using multiple analytical methods to determine its structural and chemical composition. At lower hydrothermal temperatures (410–420 °C) the wax resembled hard paraffin while at higher temperatures (430–440 °C) it exhibited diesel-like characteristics. It was found that temperature significantly influenced the morphology and properties of hydrothermal wax from PE, even with a temperature variation of 5 °C. The wax obtained at 425 °C showed optimal viscosity and solubility, facilitating further processing. That is the reason that the addition of different solvent

on the wax derived at 425 °C have been extensively studied. For instance, the addition of C_2H_5OH or CH_3COOH promoted PE chain splitting. In particular, C_2H_5OH addition specifically enhanced the cyclization, branching, and aromatization of the products. In the case of H_2O_2 addition, which promoted an oxygen environment, more disordered product distributions were obtained.

This work reported the hydrothermal conversion of PE for wax production, providing a foundation for the quantitative analysis and upgrading of hydrothermal wax and addressing the urgent challenge of plastic waste management. However, for waxes obtained at lower temperatures, the characterization methods employed in this study could not fully reveal their composition. These waxes, with morphology, structure, and hardness similar to paraffin, may serve as raw materials for phase-change materials. For softer paraffin, applications could be expanded by introducing oxygen-containing functional groups, enabling the production of soaps, surfactants, and related products. The potential of these possibilities will be investigated in greater depth in further research. In conclusion, the novel approach to plastic waste management by employing an optimal hydrothermal conversion is going to reduce environmental risk.

Declaration of Competing Interest

The authors declare that they have no known competing financial interests or personal relationships that could have appeared to influence the work reported in this paper.

Acknowledgments

This work was supported by the European Union HORIZON TMA MSCA Staff Exchanges program (HORIZON-MSCA-2021-SE-01) under Grant Agreement No. 101086071, as part of the project “CUPOLA – Carbon-neutral pathways of recycling marine plastic waste.” Financial support was further provided by the National Natural Science Foundation of China (Grant No. 52125601). Additional funding was provided by the Ministry of Science and Higher Education

in Poland through the "PMW" program (Grant Agreement No. 5863/HE/2024/2, Project No.

The authors also acknowledge the technical assistance provided by the Analytical and Testing

Center of Huazhong University of Science & Technology (http://atc.hust.edu.cn).

References

Statistica, 2024. Annual production of plastics worldwide from 1950 to 2023.https://doi.org/https://www.statista.com/statistics/282732/global-production-of-plastics-since-1950/

Abdy, C., Zhang, Y., Wang, J., Yang, Y., Artamendi, I., Allen, B., 2022. Pyrolysis of polyolefin plastic waste and potential applications in asphalt road construction: A technical review. Resources, Conservation and Recycling 180, 106213.https://doi.org/https://doi.org/10.1016/j.resconrec.2022.106213

Al-Salem, S.M., Dutta, A., 2021. Wax Recovery from the Pyrolysis of Virgin and Waste Plastics. Industrial & Engineering Chemistry Research 60, 8301-8309.https://doi.org/10.1021/acs.iecr.1c01176

Al-Salem, S.M., Lettieri, P., 2010. Kinetic study of high density polyethylene (HDPE) pyrolysis. Chemical Engineering Research and Design 88, 1599-1606.https://doi.org/10.1016/j.cherd.2010.03.012

Andrady, A.L., Neal, M.A., 2009. Applications and societal benefits of plastics. Philosophical transactions of the Royal Society of London. Series B, Biological sciences 364, 1977-1984.https://doi.org/10.1098/rstb.2008.0304

Artetxe, M., Lopez, G., Amutio, M., Elordi, G., Bilbao, J., Olazar, M., 2013. Cracking of High Density Polyethylene Pyrolysis Waxes on HZSM-5 Catalysts of Different Acidity. Industrial & Engineering Chemistry Research 52, 10637-10645.https://doi.org/10.1021/ie4014869

Babij, N.R., McCusker, E.O., Whiteker, G.T., Canturk, B., Choy, N., Creemer, L.C., Amicis, C.V.D., Hewlett, N.M., Johnson, P.L., Knobelsdorf, J.A., Li, F., Lorsbach, B.A., Nugent, B.M., Ryan, S.J., Smith, M.R., Yang, Q., 2016. NMR Chemical Shifts of Trace Impurities: Industrially Preferred Solvents Used in Process and Green Chemistry. Organic Process Research & Development 20, 661-667.https://doi.org/10.1021/acs.oprd.5b00417

Barbarias, I., Artetxe, M., Lopez, G., Arregi, A., Bilbao, J., Olazar, M.J.F.P.T., 2018. Influence of the conditions for reforming HDPE pyrolysis volatiles on the catalyst deactivation by coke. 171, 100-109.https://doi.org/10.1016/j.fuproc.2017.11.003.

Bray, D.J., Anderson, R.L., Warren, P.B., Lewtas, K., 2020. Wax Formation in Linear and Branched Alkanes with Dissipative Particle Dynamics. Journal of Chemical Theory and Computation 16, 7109-7122.https://doi.org/10.1021/acs.jctc.0c00605

Chang, X., Fang, Y., Wang, Y., Wang, F., Shang, L., Zhong, R., 2022. Microplastic pollution in soils, plants, and animals: A review of distributions, effects and potential mechanisms. The Science of the total environment 850, 157857.https://doi.org/10.1016/j.scitotenv.2022.157857

Cheng, Y., Ekici, E., Yildiz, G., Yang, Y., Coward, B., Wang, J., 2023. Applied machine learning for prediction of waste plastic pyrolysis towards valuable fuel and chemicals production. Journal of Analytical and Applied Pyrolysis 169, 105857.https://doi.org/https://doi.org/10.1016/j.jaap.2023.105857

Cookson, D.J., Latten, J.L., Shaw, I.M., Smith, B.E., 1985. Property-composition relationships for diesel and kerosene fuels. Fuel 64, 509-519.https://doi.org/10.1016/0016-2361(85)90086-9

Derraik, J.G.B., 2002. The pollution of the marine environment by plastic debris: a review. Marine Pollution Bulletin 44, 842-852.https://doi.org/10.1016/S0025-326X(02)00220-5

Ding, H., Hesp, S.A.M., 2021. Balancing the Use of Wax-Based Warm Mix Additives for Improved Asphalt Compaction with Long-Term Pavement Performance. ACS Sustainable Chemistry & Engineering 9, 7298-7305.https://doi.org/10.1021/acssuschemeng.1c01242
Dutta, A., 2017. Chapter 4 - Fourier Transform Infrared Spectroscopy, in: Thomas, S., Thomas, R., Zachariah, A.K., Mishra, R.K. (Eds.), Spectroscopic Methods for Nanomaterials Characterization. Elsevier, pp. 73-93.
Fivga, A., Dimitriou, I., 2018. Pyrolysis of plastic waste for production of heavy fuel substitute: A techno-economic assessment. Energy 149, 865-874.https://doi.org/10.1016/j.energy.2018.02.094
Hendrickson, T.P., Bose, B., Vora, N., Huntington, T., Nordahl, S.L., Helms, B.A., Scown, C.D., 2024. Paths to circularity for plastics in the United States. One Earth 7, 520-531.https://doi.org/10.1016/j.oneear.2024.02.005
Huang, H., Wang, X., Yu, J., Chen, Y., Ji, H., Zhang, Y., Rehfeldt, F., Wang, Y., Zhang, K., 2019. Liquid-Behaviors-Assisted Fabrication of Multidimensional Birefringent Materials from Dynamic Hybrid Hydrogels. ACS Nano 13, 3867-3874.https://doi.org/10.1021/acsnano.9b00551
Jung, M.R., Horgen, F.D., Orski, S.V., Rodriguez C, V., Beers, K.L., Balazs, G.H., Jones, T.T., Work, T.M., Brignac, K.C., Royer, S.-J., Hyrenbach, K.D., Jensen, B.A., Lynch, J.M., 2018. Validation of ATR FT-IR to identify polymers of plastic marine debris, including those ingested by marine organisms. Marine Pollution Bulletin 127, 704-716.https://doi.org/10.1016/j.marpolbul.2017.12.061
Khatun, R., Xiang, H., Yang, Y., Wang, J., Yildiz, G., 2021. Bibliometric analysis of research trends on the thermochemical conversion of plastics during 1990–2020. Journal of Cleaner Production 317, 128373.https://doi.org/https://doi.org/10.1016/j.jclepro.2021.128373
Kongngoen, P., Phetwarotai, W., Assabumrungrat, S., Phusunti, N., 2023. Possible use of spent FCC catalyst for upgrading of wax from the pyrolysis of plastics to liquid fuel. Journal of Analytical and Applied Pyrolysis 173, 106076.https://doi.org/10.1016/j.jaap.2023.106076
Li, C., Wang, H., Fu, C., Shi, S., Li, G., Liu, Q., Zhou, D., Jiang, L., Cheng, Y., 2023. Evaluation of modified bitumen properties using waste plastic pyrolysis wax as warm mix additives. Journal of Cleaner Production 405, 136910.https://doi.org/10.1016/j.jclepro.2023.136910
Liu, J., Li, Y., Deng, W., Wu, Y., Chen, D., Zhang, X., Liu, X., Han, L., 2025. Study on a potential bone char catalyst for high efficiency catalytic pyrolysis of polypropylene plastic. Fuel 381, 133625.https://doi.org/10.1016/j.fuel.2024.133625
Liu, Q., Jiang, D., Zhou, H., Yuan, X., Wu, C., Hu, C., Luque, R., Wang, S., Chu, S., Xiao, R., Zhang, H., 2023. Pyrolysis–catalysis upcycling of waste plastic using a multilayer stainless-steel catalyst toward a circular economy. 120, e2305078120.https://doi.org/doi:10.1073/pnas.2305078120
Maqsood, T., Dai, J., Zhang, Y., Guang, M., Li, B., 2021. Pyrolysis of plastic species: A review of resources and products. Journal of Analytical and Applied Pyrolysis 159, 105295.https://doi.org/10.1016/j.jaap.2021.105295
Missau, J., Rocha, J.d.G.d., Dotto, G.L., Bertuol, D.A., Ceron, L.P., Tanabe, E.H., 2018. Purification of crude wax using a filter medium modified with a nanofiber coating. Chemical Engineering Research and Design 136, 734-743.https://doi.org/10.1016/j.cherd.2018.06.031
Movasaghi, Z., Rehman, S., ur Rehman, D.I.J.A.S.R., 2008. Fourier Transform Infrared (FTIR) Spectroscopy of Biological Tissues. 43, 134 - 179.https://doi.org/10.1080/05704920701829043
Nayanathara Thathsarani Pilapitiya, P.G.C., Ratnayake, A.S., 2024. The world of plastic waste: A review. Cleaner Materials 11, 100220.https://doi.org/10.1016/j.clema.2024.100220

Norouzi, O., Haddadi, S.A., Salaudeen, S., Soltanian, S., Bartocci, P., Arjmand, M., Dutta, A., 2024. Catalytic upgrading of polyethylene plastic waste using GMOF catalyst: Morphology, pyrolysis, and product analysis. Fuel 369, 131742.https://doi.org/10.1016/j.fuel.2024.131742
Patil, P.B., Goswami, A.D., Pinjari, D.V., 2024. Development of industrial-grade grease from waste pyrolysis wax. Journal of the Indian Chemical Society 101, 101190.https://doi.org/10.1016/j.jics.2024.101190
Prus, Z., Wilk, M., 2024. Microplastics in Sewage Sludge: Worldwide Presence in Biosolids, Environmental Impact, Identification Methods and Possible Routes of Degradation, Including the Hydrothermal Carbonization Process. 17, 4219.https://doi.org/https://www.mdpi.com/1996-1073/17/17/4219
Qiao, Y., Xu, F., Xu, S., Yang, D., Wang, B., Ming, X., Hao, J., Tian, Y., 2018. Pyrolysis Characteristics and Kinetics of Typical Municipal Solid Waste Components and Their Mixture: Analytical TG-FTIR Study. Energy & Fuels 32, 10801-10812.https://doi.org/10.1021/acs.energyfuels.8b02571
Rudyk, S., Ongarbayev, Y., Spirov, P., 2023. Feature selection in GC-MS, NMR and MALDI-TOF spectra of tar sand bitumen. Unconventional Resources 3, 61-71.https://doi.org/https://doi.org/10.1016/j.uncres.2022.12.005
Sarma, H., Hazarika, R.P., Kumar, V., Roy, A., Pandit, S., Prasad, R.J.E.S., 2022. Microplastics in marine and aquatic habitats: sources, impact, and sustainable remediation approaches. 5, 39 - 49.https://doi.org/10.1016/j.scitotenv.2022.157857.
Speight, R.J., Rourke, J.P., Wong, A., Barrow, N.S., Ellis, P.R., Bishop, P.T., Smith, M.E., 2011. 1H and 13C solution- and solid-state NMR investigation into wax products from the Fischer–Tropsch process. Solid State Nuclear Magnetic Resonance 39, 58-64.https://doi.org/10.1016/j.ssnmr.2011.03.008
Wang, J., Ma, Y., Li, S., Yue, C., 2023. Study of HDPE plastic pyrolysis characteristics using high pressure autoclave. Journal of the Energy Institute 108, 101244.https://doi.org/10.1016/j.joei.2023.101244
Xu, Z., Munyaneza, N.E., Zhang, Q., Sun, M., Posada, C., Venturo, P., Rorrer, N.A., Miscall, J., Sumpter, B.G., Liu, G., 2023. Chemical upcycling of polyethylene, polypropylene, and mixtures to high-value surfactants. 381, 666-671.https://doi.org/10.1126/science.adh0993
Yang, Y., Wang, G., Lei, S., Xiao, H., Yang, H., Chen, H., 2024. Coupling dechlorination and catalytic pyrolysis to produce carbon nanotubes from mixed polyvinyl chloride and polyethylene. Waste Management 178, 97-104.https://doi.org/10.1016/j.wasman.2024.02.004
Zhang, F., Zhao, Y., Wang, D., Yan, M., Zhang, J., Zhang, P., Ding, T., Chen, L., Chen, C., 2021. Current technologies for plastic waste treatment: A review. Journal of Cleaner Production 282, 124523.https://doi.org/10.1016/j.jclepro.2020.124523